


Article

Combustion Characteristics, Kinetics and Thermodynamics of Peanut Shell for Its Bioenergy Valorization

Jialiu Lei ^{1,2,*} , Xiaoyu Liu ¹, Biao Xu ¹, Zicong Liu ¹ and Yongjun Fu ¹

¹ School of Materials Science and Engineering, Hubei Polytechnic University, Huangshi 435003, China; lxy2970844493@icloud.com (X.L.); xubiao@stu.hbpu.edu.cn (B.X.); liuzicong@stu.hbpu.edu.cn (Z.L.); fuyongjun@hbpu.edu.cn (Y.F.)

² The State Key Laboratory of Refractories & Metallurgy, Wuhan University of Science and Technology, Wuhan 430081, China

* Correspondence: lejialiu@hbpu.edu.cn; Tel.: +86-0714-635-8328

Abstract: To realize the utilization of peanut shell, this study investigates the combustion behavior, chemical kinetics and thermodynamic parameters of peanut shell using TGA under atmospheric air at the heating rates of 10, 20, and 30 K/min. Results indicate that increasing the heating rate leads to higher ignition, burnout, and peak temperatures, as observed in the TG/DTG curves shifting to the right. Analysis of combustion performance parameters suggest that higher heating rates can enhance combustion performances. Kinetic analysis using two model-free methods, KAS and FWO, shows that the activation energy (E_a) ranges from 93.30 to 109.65 kJ/mol for FWO and 89.72 to 103.88 kJ/mol for KAS. The data fit well with coefficient of determination values (R^2) close to 1 and the mean squared error values (MSE) less than 0.006. Pre-exponential factors using FWO range from 2.19×10^6 to $8.08 \times 10^7 \text{ s}^{-1}$, and for KAS range from 9.72×10^5 to $2.25 \times 10^7 \text{ s}^{-1}$. Thermodynamic analysis indicates a low-energy barrier ($\leq \pm 6 \text{ kJ/mol}$) between activation energy and enthalpy changes, suggesting easy reaction initiation. Furthermore, variations in enthalpy (ΔH), Gibbs free energy (ΔG), and entropy (ΔS) upon conversion (α) suggest that peanut shell combustion is endothermic and non-spontaneous, with the generation of more homogeneous or well-ordered products as combustion progresses. These findings offer a theoretical basis and data support for the further utilization of agricultural biomass.



Citation: Lei, J.; Liu, X.; Xu, B.; Liu, Z.; Fu, Y. Combustion Characteristics, Kinetics and Thermodynamics of Peanut Shell for Its Bioenergy Valorization. *Processes* **2024**, *12*, 1022. <https://doi.org/10.3390/pr12051022>

Academic Editors: Jacek Grams and Agnieszka Ruppert

Received: 21 April 2024

Revised: 13 May 2024

Accepted: 15 May 2024

Published: 17 May 2024



Copyright: © 2024 by the authors. Licensee MDPI, Basel, Switzerland. This article is an open access article distributed under the terms and conditions of the Creative Commons Attribution (CC BY) license (<https://creativecommons.org/licenses/by/4.0/>).

Keywords: combustion characteristics; kinetics and thermodynamics; thermogravimetric analysis; isoconversional methods; peanut shell

1. Introduction

Biomass is widely adopted as a renewable energy source with high sustainability. Its diverse sources include forestry, agriculture, organic waste, and livestock and poultry manure [1,2]. Through thermochemical processes such as pyrolysis, gasification, and combustion, biomass can be transformed into valuable energy [3]. Notably, biomass is considered a carbon-neutral energy source, capable of achieving zero carbon emissions and mitigating greenhouse gas effects, particularly those of carbon dioxide [4,5]. With stringent requirements to reduce carbon emissions, China aims to run carbon reduction plans by 2030 and achieve carbon neutrality by 2060 [6,7]. To this end, the development of biomass energy is of significant importance. By reducing reliance on fossil fuels and addressing environmental concerns, biomass energy holds significant potential. Accordingly, numerous investigations have been conducted focusing on biomass energy to enhance global energy structures while meeting stringent carbon emission regulations.

Applications of biomass mainly include combustion directly or indirectly as fuel or the production of charcoal, bio-oil, tar, and gas by pyrolysis technology. The content of sulfur and nitrogen in biomass is low, and the emission of SO_x and NO_x in the combustion process is less, which contributes to good emission characteristics. After combustion, there is less

ash, and the generated ash contains a large amount of organic potassium salt, which can be used to recover and extract potash fertilizer, greatly reducing the sites of ash stacking and reducing the cost of ash disposal and resource waste [8]. Therefore, based on the advantages of low cost, low risk, and high efficiency of biomass, biomass power generation is one of the most promising utilization technologies and can generate efficient and clean electric energy by direct combustion or gasification after simple treatment of collected biomass as raw materials. Promoting the deepening development of biomass energy will help increase the supply of high-quality energy, ease the pressure on domestic coal power generation, and play an important guiding role in improving energy consumption structures and the ecological environment.

Peanut shells represent a substantial agricultural waste in key peanut-producing countries like China, Vietnam, and Indonesia. China, as the world's largest peanut producer, produces 17 million tons of peanuts, accounting for more than 40% of the world's total production. The production of peanut shells is as high as 5 million tons, some of which are used as fuel, most of which are piled up or directly burned, wasting substantial resources [9]. Hence, exploring the utilization potential of peanut shells has become a hot research topic in recent years. In this context, understanding the combustion features and thermal characteristics of solid fuel in depth is crucial for designing combustion equipment on an industrial scale [10,11].

Methods for addressing the dynamic parameters of the combustion process are primarily categorized into model-fitting and model-free methods [12–14]. In the former methods, kinetic parameters are calculated by assuming a model for each reaction, and then finding the best fit of the data to the model. These methods mainly adopt the method of a single heating rate, and thus the kinetic parameters obtained are not applicable, and often cannot predict the reaction process under other heating rate conditions. This makes model-fitting methods under a single heating rate limited to some extent. The latter methods, on the other hand, calculate the kinetic parameters at the same conversion from several pyrolysis curves with different heating rates. In this approach, variations in the activation energy with conversion rate can be determined using the isoconversion rate method, which can reveal the nature of some seemingly simple reactions that are complex.

Up to now, numerous studies about the kinetic and thermodynamic parameters of peanut shell degradation have been carried out under inert atmosphere. Torres-García et al. applied thermogravimetric analysis to calculate the activation energy of peanut shell upon the conversion degree during the pyrolysis process, and judged that the pyrolytic pathway of the main pseudo-components in peanut shell was independent of the heating rate [15]. Kumar et al. studied the thermal degradation behaviors of peanut shell in an inert atmosphere, and the activation energy was estimated suitably by isoconversional methods [16]. Varma et al. explored the pyrolysis behavior of peanut shell in a N₂ atmosphere, and the kinetic and thermodynamic parameters were revealed [17]. Tao et al. utilized thermogravimetric-mass spectrometry to elucidate the pyrolytic reaction mechanism of peanut shell and found that the results of the thermodynamic and kinetic parameters were matched well in model-free methods [18]. To the best of our knowledge, few studies have focused on the combustion behaviors of peanut shell [19,20]. Despite a significant amount of research on this subject for other biomasses, the effects of heating rates on the combustion performance and kinetic and thermodynamic parameters of peanut shell in an air environment need further exploration. In addition, recently published papers have dealt with both model-free and model-fitting methods to characterize the kinetics of different biomasses and biowastes [11,21–24]. However, due to the basic known fact that biomass is mainly composed of hemicellulose, cellulose, and lignin, the total combustion process cannot be characterized by a single reaction model/mechanism. Thus, the model-free methods are more adaptable regarding combustion kinetics and thermodynamics analysis.

This paper aims to explore the thermochemical conversion of peanut shells during combustion. Through a combination of experimental analysis and theoretical approaches, thermogravimetric analysis is conducted to examine the combustion characteristics of raw

peanut shell materials under atmospheric air. This study employs two model-free kinetic methods, namely the Kissinger–Akahira–Sunose (KAS) and Flynn–Wall–Ozawa (FWO) methods, to explore the combustion kinetics parameters. Additionally, a thermodynamic analysis is carried out. The findings of this study can offer valuable insights for the design, transformation, and operational optimization of combustion equipment, thereby facilitating the efficient and clean utilization of peanut shells.

2. Materials and Methods

2.1. Materials

The peanut shells utilized in this experimental investigation originated from Hubei province, China. These samples were grounded using a 150-mesh sieve. In order to avoid internal and external heat and mass transfer limitations, the peanut shell particles with a size of 74–106 μm were collected, according to Brems et al. [25] and Van de Velden et al. [26,27]. Subsequently, the finely ground samples were dried at 373 K for 24 h.

The proximate analysis of the peanut shell was conducted following the GB/T212–2008 standard [28]. For the ultimate analysis, a CHNS/O analyzer was employed, which simultaneously detected the weight percentage of carbon, hydrogen, nitrogen, and sulfur in the samples. The weight percentage of oxygen was determined by the difference. Each experiment was repeated twice, and the average values were recorded. The higher heating value (HHV) of peanut shell is very important for carrying out the energy analysis. Its value can be estimated by correlation based on proximate analysis [29]. The results of the proximate, ultimate analyses and HHV of the peanut shell are summarized in Table 1. The significant volatile and fixed carbon content indicates the potential of peanut shells as a fuel source in thermochemical processes. The low nitrogen and sulfur content in the ultimate analysis is advantageous as it leads to lower emissions of toxic NO_x and SO_x during conversion processes, making peanut shells a promising alternative for bioenergy production regarding environmental sustainability and high volatility [30].

Table 1. Proximate, ultimate analyses and HHV of peanut shell.

Proximate Analysis/%				Ultimate Analysis/%					HHV (MJ/kg)
Moisture	Fixed Carbon	Volatiles	Ash	C	H	N	S	O	
8.16	14.38	57.20	20.26	34.97	5.33	0.54	0.01	59.69	13.39

2.2. Experimental Procedures

Thermogravimetric testing was conducted using a thermogravimetric analyzer (TGA5500, Waters, Milford, MA, USA). Each sample, weighing approximately 6 ± 0.5 mg, was placed in an alumina crucible. The samples were then heated at various rates: 10, 20, and 30 K/min, starting from room temperature and reaching 1073 K, under atmospheric air with a flow rate of 100 mL/min. The selection of the range of heating rates was mainly based on the actual heating rate of biomass power generation boilers. The real-time change in mass loss was monitored throughout the entire process. To enhance accuracy, each test was performed in triplicate to minimize vibration errors.

2.3. Combustion Characteristic Parameters

To explore the oxidative decomposition of peanut shells, it is crucial to explore the characteristic temperature, characteristic time, and weight loss rate from the TG/DTG curve during the combustion process.

2.3.1. Characteristic Temperature and Characteristic Time

The ignition temperature (T_i) represents the minimum temperature at which the fuel ignites spontaneously without an external source. Typically, the ignition temperature is determined using the TG-DTG tangent method [31]. This method involves drawing a vertical line on the X-axis at the maximum peak of the DTG curve and intersecting the

TG curve at a point. Subsequently, a tangent line is drawn on the TG curve after this point. When the tangent line intersects with a parallel line parallel to the X-axis, it indicates the point at which the TG begins to lose weight. The temperature corresponding to this point is the ignition temperature (T_i), and the time corresponding to reaching the ignition temperature is the ignition time (t_i).

The burnout temperature (T_b) represents the temperature at which the combustion of the sample ceases, indicating the difficulty of sample burnout. It is identified when the TG curve approaches a horizontal line and the DTG curve approaches 0, signifying that the fuel combustion is essentially complete. In this study, the burnout temperature is defined as the point where the weight loss at the terminal phase of the TG profile reaches 98% [32]. The time corresponding to reaching the burnout temperature is referred to as the burnout time (t_b).

The initial release temperature of volatile matter (T_v) is defined as the temperature corresponding to a mass loss rate of 0.1 mg/min [33]. The peak temperature (T_m) refers to the temperature of the maximum weight loss peak in the DTG curve during the combustion process. The time corresponding to reaching the peak temperature is t_m . $\Delta T_{1/2}$ represents the temperature interval at half the value of the peak weight loss rate in both the descending and rising parts of the DTG peak, while $\Delta t_{1/2}$ represents the time interval at half the value of the peak weight loss rate.

2.3.2. Weight Loss Rate

The maximum combustion rate (v_{\max}) refers to the highest weight loss rate of the fuel during combustion, indicating the intensity of the fuel combustion reaction. A higher maximum combustion rate suggests a more vigorous release of volatile matter, leading to a faster weight loss rate after ignition, typically associated with a lower corresponding temperature. Meanwhile, v_{mean} represents the average weight loss rate of the sample throughout the entire combustion process, from the ignition temperature to the burnout temperature. A higher v_{mean} value indicates a more intense overall combustion process.

2.3.3. Combustion Performance Parameters

To assess the combustion characteristics of peanut shells, several parameters were utilized in this study: volatile matter release (D_v), ignition index (D_i), burnout index (D_b), combustion intensity (H_f), combustion stability index (D_{si}), and comprehensive combustibility (S). These parameters are defined in terms of characteristic temperature, characteristic time, and weight loss rate. Relevant expressions of combustion performance parameters are described as follows [34–36]:

$$D_v = \frac{-v_{\max}}{T_m \times T_v \times \Delta T_{1/2}} \quad (1)$$

$$D_i = \frac{-v_{\max}}{t_m \times t_i} \quad (2)$$

$$D_b = \frac{-v_{\max}}{t_m \times t_b \times \Delta t_{1/2}} \quad (3)$$

$$H_f = 10^{-3} \times T_m \times \ln \left(\frac{\Delta T_{1/2}}{-v_{\max}} \right) \quad (4)$$

$$D_{\text{si}} = 8.5875 \times 10^7 \times \frac{-v_{\max}}{T_m \times T_i} \quad (5)$$

$$S = \frac{(-v_{\max}) \times (-v_{\text{mean}})}{T_i^2 \times T_b} \quad (6)$$

2.4. Kinetic Method

The kinetics analysis plays a crucial role in understanding the reaction process of biomass. As recommended by the Kinetics Committee of the International Confederation for Thermal Analysis and Calorimetry [37], this article employs model-free methods like FWO and KAS to compute the kinetic parameters. The solid–gas reaction rate is defined as follows:

$$\frac{d\alpha}{dt} = k(T)f(\alpha) \quad (7)$$

where α represents the conversion degree, t denotes the combustion time, $k(T)$ stands for the reaction rate constant, and $f(\alpha)$ represents the differential expression of the reaction model. The α during the combustion process can be obtained from thermogravimetric analysis data, as follows:

$$\alpha = \frac{m_0 - m_t}{m_0 - m_\infty} \quad (8)$$

where m_0 , m_t , and m_∞ are the initial, instant, and residual mass of biomass during the combustion process, respectively. Based on the Arrhenius law, $k(T)$ can be obtained using the following expression:

$$k(T) = A \exp\left(-\frac{E_\alpha}{RT}\right) \quad (9)$$

where T represents the combustion temperature, A is the pre-exponential factor, E_α is the activation energy, and R represents the universal gas constant. Combining Equations (7) and (9) at a given constant ($\beta = dT/dt$) and rearranging yields Equation (10):

$$\frac{d\alpha}{dT} = \frac{A}{\beta} \exp\left(-\frac{E_\alpha}{RT}\right) f(\alpha) \quad (10)$$

The integral form of $f(\alpha)$ can be presented as:

$$\int_0^\alpha \frac{d\alpha}{f(\alpha)} = g(\alpha) = \frac{A}{\beta} \int_{T_0}^T e^{-\frac{E_\alpha}{RT}} dT \quad (11)$$

2.4.1. The FWO Method

The FWO approach utilizes Doyle's approximation for temperature integration and is formulated as Equation (12) [38,39]. It is worth noting that E_α can be determined from the gradient $-1.052E_\alpha/R$ of the regression lines.

$$\ln\beta = \ln \frac{AE_\alpha}{g(\alpha)R} - 5.331 - 1.052 \frac{E_\alpha}{RT} \quad (12)$$

2.4.2. The KAS Method

The KAS technique is expressed by Equation (13) [40]. E_α can be derived from the slope $-E_\alpha/R$ of the regression lines.

$$\ln \frac{\beta}{T^2} = \ln \frac{AE_\alpha}{g(\alpha)R} - \frac{E_\alpha}{RT} \quad (13)$$

It should be noted in particular that, due to the complexity of biomass composition, the total combustion process cannot be characterized by a single-step formulation. If the activation energy has little change in a certain conversion degree range, then a deeper insight concerning the potential variation of E_α with the conversion degree is applicable to this corresponding conversion degree range.

2.5. Thermodynamic Method

Based on E_α computed using the FWO and KAS methods, the pre-exponential factor A , as well as thermodynamic parameters like change in enthalpy (ΔH), change in Gibbs free energy (ΔG), and change in entropy (ΔS) at a specific heating rate, can be determined as follows [41,42]:

$$A = \frac{\beta E_\alpha \exp\left(\frac{E_\alpha}{RT_m}\right)}{RT_m^2} \quad (14)$$

$$\Delta H = E_\alpha - RT \quad (15)$$

$$\Delta G = E_\alpha + RT_m \ln\left(\frac{K_B T_m}{hA}\right) \quad (16)$$

$$\Delta S = \frac{\Delta H - \Delta G}{T_m} \quad (17)$$

In these equations, the values of A at each conversion degree can be obtained from Kissinger's method [43]. $k_B = 1.381 \times 10^{-23}$ J/K represents the Boltzmann constant and $h = 6.626 \times 10^{-34}$ J/s is Planck's constant.

3. Results and Discussion

3.1. Thermogravimetric Analysis

Figure 1 illustrates the TG and DTG profiles of peanut shells from room temperature to 1073 K at three different heating rates. Focusing on the TG and DTG curves obtained at a heating rate of 20 K/min, distinct combustion stages are evident. Initially, there is a stage corresponding to water evaporation (ambient to 440 K), primarily involving the release of bound water within the peanut shells. This stage is characterized by a minor decrease in the TG curve and a low weight loss rate, constituting approximately 7.68% of the total weight loss, closely aligning with the water content indicated in Table 1. The subsequent stage, spanning from 440 K to 832 K, represents the main combustion phase, exhibiting the highest weight loss rate and accounting for 72.39% of the total weight loss. Notably, this stage is marked by a significant decline in weight on the TG curve, accompanied by two distinct peaks on the DTG curve. The first peak corresponds to the combustion of volatile components, occurring at approximately 584.60 K. These weight losses primarily result from the thermal degradation and combustion of volatile substances such as hemicelluloses, celluloses, and certain lignin components [44]. The second peak corresponds to the combustion of residual volatiles and fixed carbon, with the weight loss peak occurring at 705.31 K. This stage mainly involves the combustion of lignin and fixed carbon, where the latter cannot combust until the volatile matter has been consumed, and the temperature is sufficiently elevated [45]. The maximum combustion rate is observed at the first DTG peak. The final stage, ranging from 832 K to 1073 K, is the burnout phase, during which both the TG and DTG curves stabilize and there is no further change in sample mass. After the combustion process, the residual mass amounts to 19.93%.

Table 2 presents the combustion stages and their associated weight losses throughout the entire combustion process at various heating rates. It indicates that the heating rate has minimal impact on the weight loss during stage II and the final residual at the end of the combustion. However, with an increase in heating rate, both the onset temperature of the main combustion stage and the temperature corresponding to the weight loss peak gradually rise. This observation may be attributed to the shorter residence time associated with higher heating rates, which impedes effective heat transfer. Consequently, a larger temperature differential between the surface and interior of the sample is observed, resulting in an upward shift of the overall DTG curve towards higher temperatures.

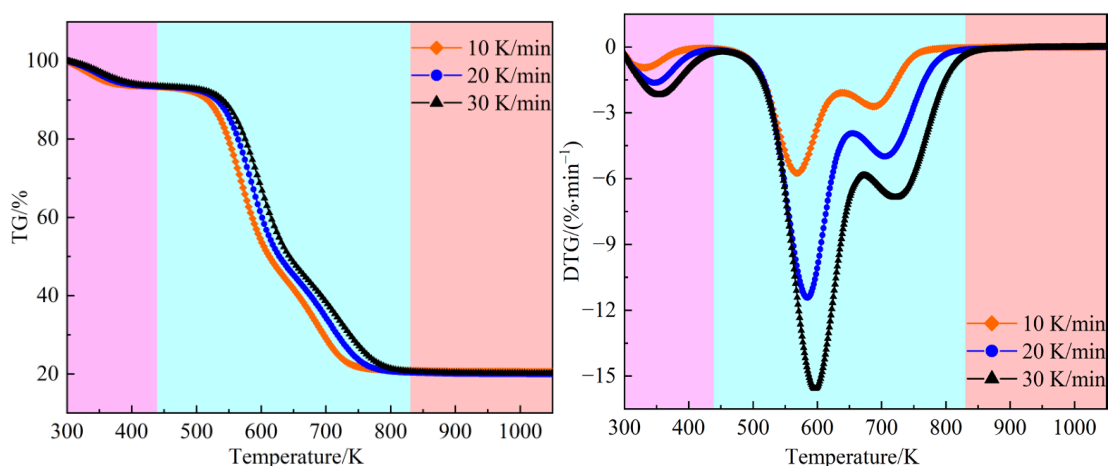


Figure 1. TG and DTG curves of the combustion process for peanut shell.

Table 2. Combustion stages and weight losses at various heating rates.

Heating Rates (K/min)	Stage I		Stage II			Stage III
	Water Evaporation		Volatile and Fixed Carbon Combustion			Burnout Stage
	Temperature Range (K)	Weight Loss (%)	Temperature Range (K)	T_m (K)	Weight Loss (%)	Residual (%)
10	299.35–423.41	7.58	423.41–799.34	568.59	72.06	20.36
20	299.22–439.84	7.68	439.84–832.14	584.60	72.39	19.93
30	298.75–452.45	7.69	452.45–842.93	596.58	72.19	20.12

3.2. Combustion Characteristic Analysis

Table 3 provides detailed outcomes outlining the influence of heating rate on combustion characteristic parameters and performance parameters for a clearer comprehension of how variations in heating rate impact combustion behavior. It is observed that alterations in heating rate exert varying degrees of influence on these characteristics. As the heating rate rises, ignition and burnout temperatures increase, alongside the maximum combustion rate and its corresponding peak temperature. The elevation of the heating rate results in a noticeable delay in the combustion reaction of the sample, hindering ignition and prolonging burnout time. The elevation in ignition temperature can be attributed to the heightened heating rate, which increases the volatilization of fuel components and decreases the residual fuel content. Consequently, the combustion reaction shifts towards higher temperature ranges. Similarly, the rise in burnout temperature is a consequence of the increased heating rate, prolonging the incomplete volatilization analysis of the sample and delaying combustion, thereby increasing the sample's burnout temperature. Moreover, the escalation in maximum combustion rate and its corresponding peak temperature signifies a more vigorous combustion capacity per unit time with the heightened heating rate. However, as the heating rate increases, the heat transfer rate may not keep pace with temperature changes, resulting in a temperature differential between the sample's surface and interior [46]. This thermal lag exacerbates the temperature gradient within the sample particles, leading to a noticeable thermal shock effect and an accelerated combustion reaction rate, thereby increasing the maximum peak temperature.

D_i and D_b align with the findings regarding ignition temperature and burnout temperature. Higher values of D_b indicate enhanced ignition performance [47,48]. This suggests that as the heating rate increases, the flammability and burnout capabilities of the fuel improve. The heightened heating rate intensifies the volatilization analysis, leading to the formation of more pores within and on the surface of the coke. This phenomenon may induce the collapse of the coke structure, resulting in increased surface area conducive to

oxygen transport to the interior of the coke and combustion of the coke surface, thereby enhancing combustion efficiency.

Table 3. Combustion parameters of peanut shells at three heating rates.

β (K min ⁻¹)	T_i (K)	T_b (K)	T_m (K)	T_v (K)	v_{max} (%·min ⁻¹)	v_{mean} (%·min ⁻¹)	D_v (%·min ⁻¹ ·K ⁻³)	D_i (%·min ⁻³)	D_b (%·min ⁻⁴)	D_{si} (%·min ⁻² ·K ⁻³)	H_f (K)	S (% ² ·min ⁻² ·K ⁻³)
10	527.85	742.54	568.59	521.11	-5.7538	-3.055	2.47×10^{-7}	0.009	0.0006	1646.30	1.49	0.85×10^{-7}
20	540.10	772.98	584.60	520.45	-11.431	-5.733	4.82×10^{-7}	0.061	0.0081	3109.03	1.12	2.91×10^{-7}
30	550.32	793.45	596.58	519.84	-15.581	-8.165	5.68×10^{-7}	0.163	0.0291	4075.55	1.04	5.29×10^{-7}

Table 3 indicates that the initial devolatilization temperature exhibits minimal change, suggesting that the heating rate slightly affects the temperature at which volatiles begin to precipitate. However, it does impact the volatile matter release index (D_v), which signifies the release performance of volatile matter in the fuel. It is also found that as the heating rate increases, the volatile matter release index increases too. A higher D_v value indicates a more centralized combustion region of char residues and higher burnout performance [49]. The comprehensive combustibility (S) encompasses various characteristics, including ignition and burnout. Utilizing the combustion index enables an evaluation of relative combustibility, offering the ability to select the most suitable option for specific conditions and purposes. A high S value indicates a high combustion reactivity of the material [50]. The combustion stability index (D_{si}) is employed to reflect the combustion stability [51]. It is observed that both the comprehensive combustibility and combustion stability index exhibit an increasing trend with the rise in heating rate. This suggests that within the discussed heating rate range, increasing the heating rate can enhance its comprehensive combustion performance and improve the stability of high combustion. Conversely, the combustion intensity (H_f) decreases with the rising heating rate. H_f characterizes the rate and intensity of the combustion process, with a smaller value indicating more efficient combustion [52]. Overall, the heating rate exhibits a positive correlation with the comprehensive combustion characteristics. However, due to variations in the degree of influence of the heating rate on different combustion indices, excessively high heating rates may induce instability and fluctuations in the combustion process of the sample.

3.3. Kinetics Analysis

The model-free methods, which do not rely on specific mechanism functions, have been commonly used for estimating more reliable activation energies (E_α). The E_α values for the combustion of peanut shells were estimated considering the conversion (α). Utilizing Equations (12) and (13), kinetics with conversions ranging from 0.10 to 0.90 at intervals of 0.05 were computed. Figure 2 illustrates the results.

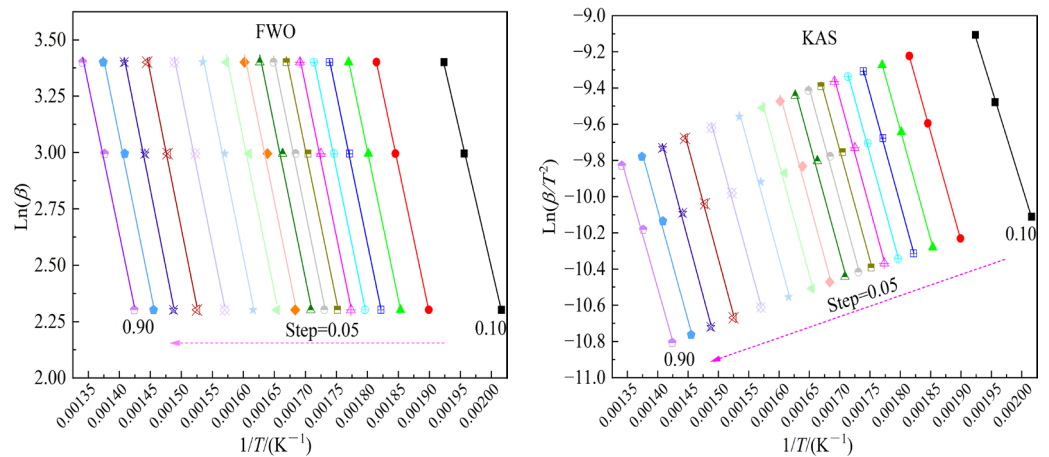


Figure 2. Combustion kinetics fitted by the FWO and KAS methods.

Table 4 reveals the E_α values together with the A values at various heating rates in the conversion degree range of 0.10 to 0.90. All correlations demonstrate statistical sufficiency, with coefficient of determination values (R^2) ranging from 0.9901 to 1.0 and mean squared error values (MSE) less than 0.006, verifying the accuracy of the outcomes.

Table 4. Kinetic parameters obtained from the two model-free methods.

α	FWO						KAS					
	E_α (kJ/mol)	R^2	MSE	$A/(s^{-1})$			E_α (kJ/mol)	R^2	MSE	$A/(s^{-1})$		
				10 K/min	20 K/min	30 K/min				10 K/min	20 K/min	30 K/min
0.10	93.30	0.9994	3.61×10^{-4}	2.16×10^6	2.38×10^6	2.33×10^6	89.72	0.9993	2.76×10^{-5}	9.72×10^5	1.09×10^6	1.09×10^6
0.15	102.89	0.9999	3.18×10^{-5}	1.81×10^7	1.89×10^7	1.78×10^7	99.29	0.9999	3.46×10^{-4}	8.16×10^6	8.68×10^6	8.30×10^6
0.20	104.08	0.9998	1.01×10^{-4}	2.35×10^7	2.44×10^7	2.28×10^7	100.33	0.9998	1.09×10^{-4}	1.03×10^7	1.08×10^7	1.03×10^7
0.25	105.05	1.0000	3.37×10^{-4}	2.92×10^7	3.00×10^7	2.80×10^7	101.17	0.9993	3.53×10^{-4}	1.24×10^7	1.30×10^7	1.23×10^7
0.30	105.56	0.9989	6.77×10^{-4}	3.26×10^7	3.35×10^7	3.12×10^7	101.58	0.9986	7.01×10^{-4}	1.35×10^7	1.42×10^7	1.35×10^7
0.35	106.15	0.9978	1.37×10^{-3}	3.72×10^7	3.80×10^7	3.53×10^7	102.07	0.9973	2.39×10^{-3}	1.51×10^7	1.58×10^7	1.49×10^7
0.40	105.72	0.9961	2.42×10^{-3}	3.38×10^7	3.47×10^7	3.23×10^7	101.51	0.9952	2.76×10^{-3}	1.33×10^7	1.40×10^7	1.32×10^7
0.45	106.45	0.9945	3.37×10^{-3}	3.98×10^7	4.06×10^7	3.77×10^7	102.15	0.9933	2.01×10^{-3}	1.54×10^7	1.61×10^7	1.52×10^7
0.50	106.46	0.9919	4.99×10^{-3}	3.98×10^7	4.07×10^7	3.77×10^7	102.03	0.9902	1.51×10^{-3}	1.49×10^7	1.57×10^7	1.48×10^7
0.55	106.75	0.9911	5.48×10^{-3}	4.25×10^7	4.33×10^7	4.01×10^7	102.19	0.9901	1.72×10^{-3}	1.55×10^7	1.62×10^7	1.53×10^7
0.60	107.05	0.9917	5.15×10^{-3}	4.53×10^7	4.61×10^7	4.27×10^7	102.31	0.9902	1.40×10^{-3}	1.59×10^7	1.66×10^7	1.57×10^7
0.65	107.59	0.9941	3.65×10^{-3}	5.11×10^7	5.19×10^7	4.79×10^7	102.64	0.9927	3.42×10^{-3}	1.71×10^7	1.79×10^7	1.68×10^7
0.70	107.38	0.9973	1.67×10^{-3}	4.88×10^7	4.95×10^7	4.58×10^7	102.10	0.9966	5.06×10^{-3}	1.52×10^7	1.59×10^7	1.50×10^7
0.75	108.75	0.9976	1.47×10^{-3}	6.61×10^7	6.66×10^7	6.12×10^7	103.22	0.9972	5.55×10^{-3}	1.94×10^7	2.02×10^7	1.90×10^7
0.80	109.65	0.9969	1.94×10^{-3}	8.06×10^7	8.08×10^7	7.40×10^7	103.88	0.9961	5.22×10^{-3}	2.25×10^7	2.33×10^7	2.19×10^7
0.85	107.53	0.9956	2.69×10^{-3}	5.04×10^7	5.12×10^7	4.73×10^7	101.37	0.9944	3.71×10^{-3}	1.29×10^7	1.36×10^7	1.29×10^7
0.90	104.81	0.9962	2.32×10^{-3}	2.77×10^7	2.85×10^7	2.66×10^7	98.24	0.9951	2.46×10^{-3}	6.45×10^6	6.91×10^6	6.63×10^6
Average	105.60						100.93					

3.3.1. Activation Energy Analysis

Figure 3 illustrates the variations of E_α against the conversion rate, indicating that both methods yield similar activation energy values, with slightly higher values obtained using the FWO method. These curves can be categorized into three stages: Initially, in the α range of 0.10 to 0.15, there is a slight increase in E_α values. For the KAS and FWO methods, E_α rises from 93.30 to 102.89 kJ/mol and 89.72 to 99.29 kJ/mol, respectively. The second region has a stable E_α , but a substantial decrease in the third region with a range of 0.80 to 0.90. Moreover, the E_α varies slightly with the conversion degree ranging from 0.20 to 0.70, indicating that this process can be described by one single-step reaction [53]. The mean E_α values in this stage are 106.20 kJ/mol and 101.83 kJ/mol for the FWO and KAS methods, respectively, which can be used to describe the main combustion process.

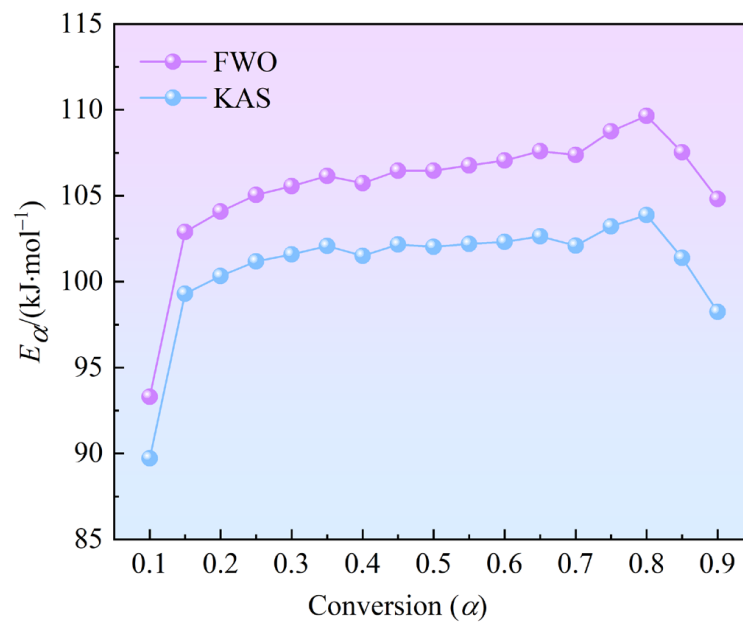


Figure 3. Distribution of activation energy (E_α) against conversion (α).

At the initial stage of the reaction, with the increase in temperature, the precipitation of volatile substances and the initial decomposition of hemicellulose and cellulose first occur. The initial decomposition requires a higher temperature and more heat to achieve its activation state, which leads to an increase in activation energy. With a further increase in temperature, the combustion process enters the main combustion stage of volatiles. At the same time, cellulose and lignin with high degrees of polymerization gradually transform into coke; the carbon structure tends to be orderly, the active site decreases, the semi-coke formed on the surface of the reactants will increase the reaction difficulty inside the reactants, and the activation energy will further increase. However, the overall increase trend is relatively gentle, with increases in amplitude of 6.6% and 4.6% for the FWO and KAS methods, respectively. E_α reaches its maximum value when α reaches 0.80. Then, the E_α gradually decreases, mainly in the combustion stage of fixed carbon. The porosity of semi-coke increases due to the volatilization and carbonization processes, and the pre-pyrolysis, aerobic cracking, and volatilization ignition processes can provide more heat, which improves the reaction activity of fixed carbon in the combustion stage, and thus the activation energy decreases.

Table 5 shows a comparison of the average activation energy in the present study with those in the literature. The mean activation energy value of peanut shell in this study is less than that of pine wood, microalgae, and tea leaves in air. The lower average activation energy suggests that the occurrence of the combustion process was easier. In addition, the mean activation energy value of peanut shell is close to that of rice husk. The minor differences in the activation energy values of different biomasses are attributed to their different pseudo-components, different experimental conditions, and different kinetic methods.

Table 5. Comparison of the average activation energy in present study and the literature.

Specimen	Average Activation Energy/(kJ/mol)	Model-Free Method	Reference
Peanut shell	105.60	FWO	This study
	100.93	KAS	
Pine wood	186.92	FWO	[54]
	186.27	Starink	
Microalgae	141.87	Starink	[55]
Tea leaves	205.15	FWO	[44]
	209.58	Friedman	
Rice husk	95.90	KAS	[56]
	101.20	FWO	

3.3.2. Pre-Exponential Factor Analysis

The parameter A is a crucial indicator of the sample's surface structure or the complexity of the combustion reaction [57]. A value lower than 10^9 s^{-1} suggests surface reactions, while A higher than 10^9 s^{-1} indicates simpler complexes with higher reactivity [58]. The results demonstrate that at various heating rates, the parameter A calculated by the FWO and KAS methods ranges from 2.16×10^6 to $8.08 \times 10^7 \text{ s}^{-1}$ and from 9.72×10^5 to $2.33 \times 10^7 \text{ s}^{-1}$, respectively. All A values fall below 10^9 s^{-1} , suggesting that the combustion process of peanut shells primarily involves surface reactions associated with a closed complex. The trend of variation in the pre-exponential factor with conversion aligns with that of the activation energy, according to the values of E_α and A demonstrated in Table 4 at different heating rates.

The E_α , $\ln A$, and corresponding values of R^2 and MSE using the FWO and KAS approaches are described in Figure 4. It is indicated that there is an intense linear relationship between the E_α and $\ln A$ values at all heating rates, which is known as the "kinetic compensation effect" [43]. The linear relationship of E_α and $\ln A$ for the combustion stage is $\ln A = 0.2116E_\alpha - 5.0766$, with the values of R^2 close to 1 and MSE close to 0. Then, the

average value of A for the main combustion stage can be computed to be $3.59 \times 10^7 \text{ s}^{-1}$ and $1.42 \times 10^7 \text{ s}^{-1}$ for the FWO and KAS approaches.

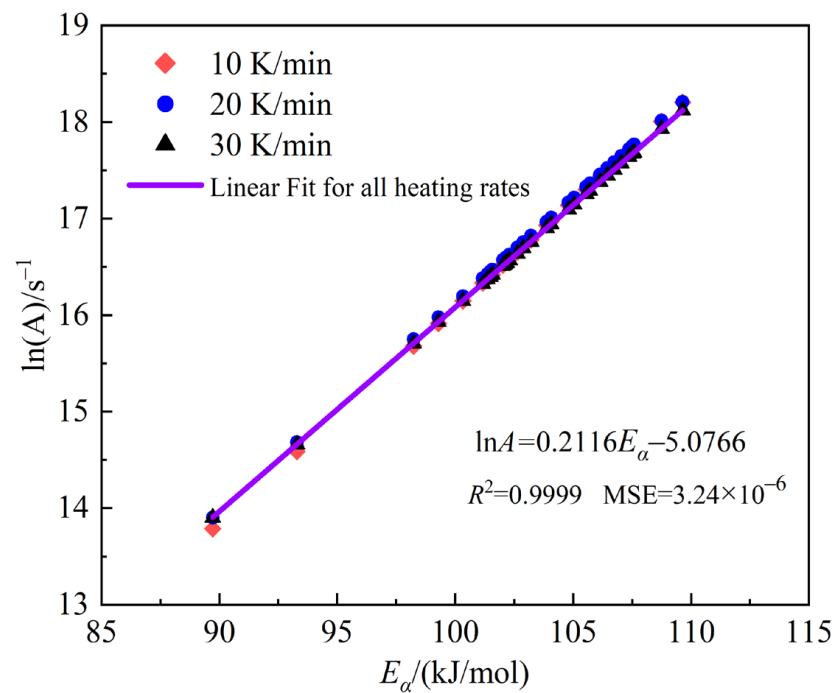


Figure 4. The kinetic compensation effect between E_α and $\ln A$.

3.4. Thermodynamic Analysis

Estimating the thermodynamic parameters of combustion is crucial for designing combustion reactors on a large scale and selecting appropriate biofuels. ΔH , ΔG , and ΔS are presented in Tables 6 and 7 at various heating rates.

Table 6. Thermodynamic properties of peanut shell obtained using the FWO method.

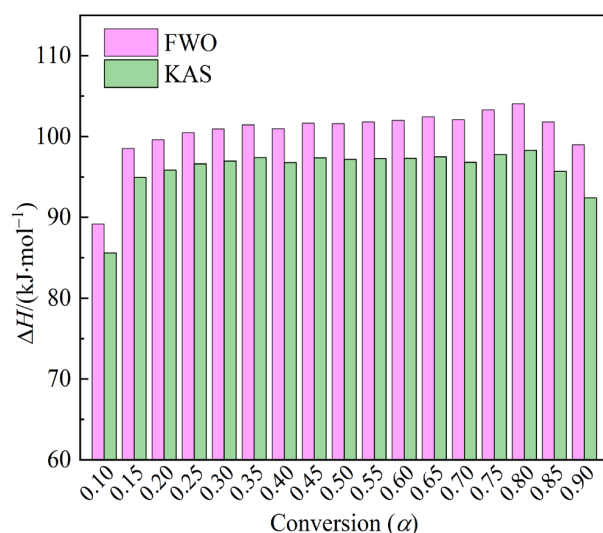
α	$\Delta H/(\text{kJ/mol})$			$\Delta G/(\text{kJ/mol})$			$\Delta S/(\text{J}/(\text{mol} \times \text{K}))$		
	10 K/min	20 K/min	30 K/min	10 K/min	20 K/min	30 K/min	10 K/min	20 K/min	30 K/min
0.10	89.18	89.05	88.98	166.66	168.39	170.13	-136.27	-135.72	-136.03
0.15	98.51	98.38	98.31	166.20	167.92	169.65	-119.05	-118.94	-119.58
0.20	99.60	99.47	99.39	166.15	167.86	169.59	-117.04	-116.99	-117.67
0.25	100.48	100.35	100.27	166.10	167.82	169.55	-115.40	-115.40	-116.13
0.30	100.93	100.80	100.71	166.08	167.79	169.52	-114.58	-114.59	-115.34
0.35	101.46	101.33	101.23	166.05	167.77	169.49	-113.61	-113.65	-114.43
0.40	100.97	100.84	100.74	166.07	167.78	169.51	-114.49	-114.51	-115.28
0.45	101.65	101.52	101.41	166.04	167.75	169.48	-113.25	-113.30	-114.10
0.50	101.60	101.46	101.35	166.04	167.75	169.48	-113.34	-113.39	-114.20
0.55	101.82	101.68	101.56	166.03	167.74	169.47	-112.93	-112.99	-113.82
0.60	102.02	101.88	101.76	166.01	167.72	169.45	-112.55	-112.63	-113.47
0.65	102.45	102.30	102.17	165.99	167.70	169.43	-111.76	-111.88	-112.73
0.70	102.08	101.92	101.79	166.00	167.71	169.44	-112.41	-112.54	-113.39
0.75	103.30	103.13	103.00	165.94	167.65	169.37	-110.16	-110.36	-111.26
0.80	104.06	103.89	103.75	165.90	167.61	169.33	-108.75	-109.00	-109.93
0.85	101.81	101.63	101.48	165.99	167.70	169.43	-112.87	-113.03	-113.90
0.90	98.97	98.77	98.61	166.11	167.83	169.56	-118.09	-118.13	-118.92
Average	100.64	100.49	100.38	166.08	167.79	169.52	-115.09	-115.12	-115.89

Table 7. Thermodynamic properties of peanut shell obtained using the KAS method.

α	$\Delta H/(\text{kJ/mol})$			$\Delta G/(\text{kJ/mol})$			$\Delta S/(\text{J}/(\text{mol} \times \text{K}))$		
	10 K/min	20 K/min	30 K/min	10 K/min	20 K/min	30 K/min	10 K/min	20 K/min	30 K/min
0.10	85.59	85.47	85.39	166.85	168.58	170.33	-142.91	-142.18	-142.37
0.15	94.92	94.79	94.71	166.37	168.09	169.82	-125.67	-125.39	-125.91
0.20	95.84	95.71	95.63	166.32	168.04	169.77	-123.96	-123.72	-124.28
0.25	96.61	96.48	96.39	166.28	168.00	169.73	-122.53	-122.34	-122.93
0.30	96.95	96.82	96.73	166.26	167.98	169.71	-121.90	-121.72	-122.34
0.35	97.38	97.25	97.15	166.24	167.96	169.69	-121.10	-120.95	-121.58
0.40	96.76	96.63	96.52	166.26	167.98	169.72	-122.24	-122.06	-122.68
0.45	97.35	97.22	97.11	166.23	167.95	169.68	-121.15	-121.00	-121.65
0.50	97.16	97.03	96.92	166.24	167.96	169.69	-121.49	-121.33	-121.98
0.55	97.25	97.11	97.00	166.23	167.95	169.68	-121.33	-121.17	-121.84
0.60	97.28	97.14	97.02	166.23	167.94	169.68	-121.25	-121.11	-121.78
0.65	97.49	97.34	97.22	166.21	167.93	169.66	-120.87	-120.75	-121.43
0.70	96.80	96.63	96.51	166.24	167.95	169.69	-122.12	-122.00	-122.66
0.75	97.77	97.59	97.46	166.19	167.90	169.63	-120.33	-120.27	-120.97
0.80	98.29	98.11	97.97	166.16	167.87	169.60	-119.37	-119.34	-120.07
0.85	95.66	95.47	95.32	166.27	167.99	169.72	-124.19	-124.05	-124.71
0.90	92.40	92.20	92.04	166.42	168.14	169.88	-130.18	-129.91	-130.48
Average	95.97	95.82	95.71	166.29	168.01	169.75	-123.68	-123.49	-124.09

As shown in Tables 6 and 7, the values of ΔH , ΔG , and ΔS at each conversion degree were nearly equal under different heating rates, indicating that the thermodynamic parameters are independent of the heating rates. Thus, in the following discussion, the thermodynamics parameters at the heating rate of 10 K/min are taken as an example.

The reaction enthalpy (ΔH) signifies the energy exchange in a chemical reaction or the energy necessary for the thermal degradation of the feedstock. The variation trend concerning conversion (α) is depicted in Figure 5. The calculated ΔH values range from 89.18 to 104.06 kJ/mol and 158.74 to 446.68 kJ/mol, with average values of 85.59 and 98.29 kJ/mol, respectively. All ΔH values corresponding to different degrees of conversion are positive, indicating the occurrence of endothermic reactions throughout the combustion process. The difference between ΔH and E_a values, lower than ± 6 kJ/mol, reflects the potential energy barrier in the process of the formation of activated complexes [59].

**Figure 5.** Variation trend of enthalpy (ΔH) upon conversion (α).

Gibbs free energy (ΔG) reflects the difficulty and direction of reactions and the total energy of the system, where a higher ΔG value indicates lower reaction favorability. Figure 6

illustrates the variations concerning conversion (α). The ΔG values calculated by the FWO and KAS methods range from 165.90 to 166.66 kJ/mol and 166.16 to 166.85 kJ/mol. The average values of ΔG for the thermal combustion of peanut shell are 166.08 kJ/mol for FWO and 166.29 kJ/mol for KAS, respectively. ΔG values at different conversions are all positive, suggesting non-spontaneous reactions in peanut shell combustion. Moreover, the values of ΔG vary within ± 1 kJ/mol corresponding to each conversion (α), indicating that peanut shell maintains a stable energy output throughout the combustion process.

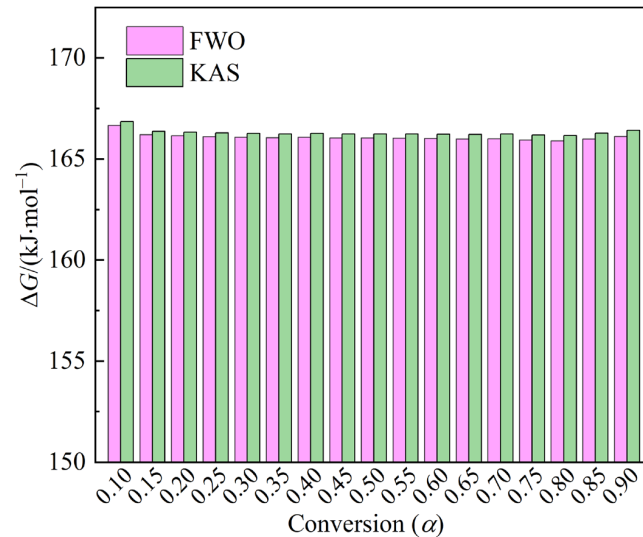


Figure 6. Variations of Gibbs free energy (ΔG) upon conversion (α).

Entropy (ΔS) is an indicator reflecting the degree of system disorder, with reaction systems exhibiting low ΔS values more readily reaching thermodynamic equilibrium. Figure 7 reveals that the entropy changes calculated by the FWO and KAS methods range from -136.27 to -108.75 J/(mol \times K) and -142.91 to -119.37 J/(mol \times K), respectively. ΔS for peanut shell falls within the negative range of -136.27 to -108.75 J/(mol \times K) and -142.91 to -119.37 J/(mol \times K) across the conversion range of 0.10–0.90, indicating proximity to thermodynamic equilibrium [60]. This range corresponds to volatile combustion and fixed carbon combustion, where a thermally stable product is produced and the degree of disorder in the products is lower than that in the reactants.

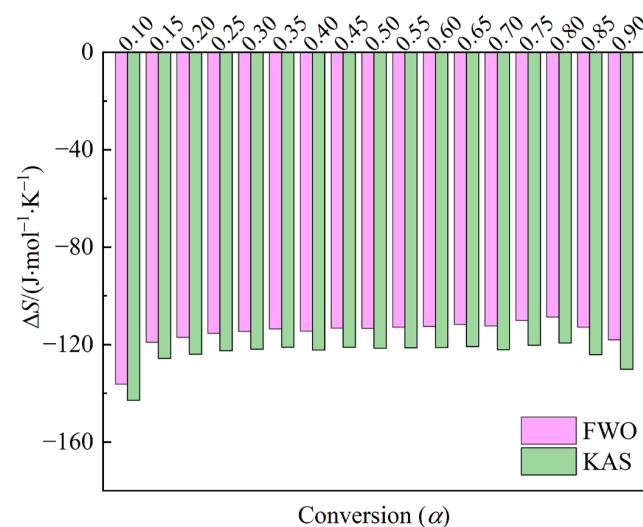


Figure 7. Variations of entropy (ΔS) upon conversion (α).

4. Conclusions

This study uses thermogravimetric analysis (TGA) to investigate combustion characteristics, kinetics, and thermodynamics parameters at three different heating rates under atmospheric air for peanut shell. The findings provide useful data for efficient combustion applications of peanut shell and promote the future design and application of large-scale combustion setups. The main achievements of this study can be summarized as follows:

(1) The combustion of peanut shell is mainly divided into three stages: the water evaporation, volatile and fixed carbon combustion, and burnout stages. As the heating rate increases, the combustion characteristic temperature of peanut shell transitions to a high-temperature zone. Meanwhile, the combustion performance parameters analyses indicate that the heating rate has an obvious influence on the combustion performance parameters.

(2) The activation energy in the conversion degree range of 0.20 to 0.70, with mean values of 106.20 kJ/mol and 101.83 kJ/mol for the FWO and KAS methods, respectively, can be used to describe the main combustion process. The linear relationship of E_α and $\ln A$ is $\ln A = 0.2116E_\alpha - 5.0766$, and the average value of A for the main combustion stage are $3.59 \times 10^7 \text{ s}^{-1}$ and $1.42 \times 10^7 \text{ s}^{-1}$ for the FWO and KAS approaches.

(3) Thermodynamic analysis reveals that the thermodynamic parameters are independent of the heating rates and the combustion of peanut shell is an endothermic and non-spontaneous process, and more homogeneous or well-ordered products are generated with the progress of combustion.

Author Contributions: Conceptualization, J.L.; methodology, J.L. and X.L.; formal analysis, J.L. and Y.F.; investigation, X.L.; data curation, B.X. and Z.L.; writing—original draft preparation, J.L.; writing—review and editing, J.L. and X.L.; supervision, Y.F. All authors have read and agreed to the published version of the manuscript.

Funding: This research was funded by the Opening Foundation of The State Key Laboratory of Refractories and Metallurgy (Wuhan University of Science and Technology), grant number G202208, and the Joint Supported by Hubei Provincial Natural Science Foundation and Huangshi of China, grant number 2023AFD010.

Data Availability Statement: The data presented in this study are available on request from the corresponding author.

Acknowledgments: The authors gratefully acknowledge the resources partially provided by the State Key Laboratory of Refractories & Metallurgy, Wuhan University of Science and Technology.

Conflicts of Interest: The authors declare no conflicts of interest.

References

- Al-Hamamre, Z.; Saidan, M.; Hararah, M.; Rawajfeh, K.; Alkhasawneh, H.E.; Al-Shannag, M. Wastes and Biomass Materials as Sustainable-renewable Energy Resources for Jordan. *Renew. Sustain. Energy Rev.* **2017**, *67*, 295–314. [[CrossRef](#)]
- Sagastume Gutiérrez, A.; Cabello Eras, J.J.; Hens, L.; Vandecasteele, C. The Energy Potential of Agriculture, Agroindustrial, Livestock, and Slaughterhouse Biomass Wastes Through Direct Combustion and Anaerobic Digestion. *Case Colombia. J. Clean. Prod.* **2020**, *269*, 122317. [[CrossRef](#)]
- Demirbaş, A. Biomass Resource Facilities and Biomass Conversion Processing for Fuels and Chemicals. *Energy Convers. Manag.* **2001**, *42*, 1357–1378. [[CrossRef](#)]
- Yang, C.; Kwon, H.; Bang, B.; Jeong, S.; Lee, U. Role of Biomass as Low-carbon Energy Source in the Era of Net Zero Emissions. *Fuel* **2022**, *328*, 125206. [[CrossRef](#)]
- Wang, R.; Song, X.L.; Liu, S.J.; Liu, Z.W. Research on Co-combustion Behaviors of Binary and Ternary Blends of Coal, Walnut Shell, and Biochar by TGA. *Processes* **2022**, *10*, 2264. [[CrossRef](#)]
- Zhao, X.; Ma, X.W.; Chen, B.Y.; Shang, Y.P.; Song, M.H. Challenges Toward Carbon Neutrality in China: Strategies and Countermeasures. *Resour. Conserv. Recycl.* **2022**, *176*, 105959. [[CrossRef](#)]
- Li, W.; Zhang, S.H.; Lu, C. Exploration of China's Net CO₂ Emissions Evolutionary Pathways by 2060 in the Context of Carbon Neutrality. *Sci. Total Environ.* **2022**, *831*, 154909. [[CrossRef](#)] [[PubMed](#)]
- Wang, Y.B.; Wang, X.B.; Tan, H.Z.; Du, W.Z.; Qu, X.D. Extraction and Quantitation of Various Potassium Salts in Straw Ash. *Environ. Prog. Sustain. Energy* **2015**, *34*, 333–338. [[CrossRef](#)]
- Yang, B.L.; Zhang, C.X.; Zhang, X.J.; Wang, G.; Li, L.; Geng, H.R.; Liu, Y. Survey of Aflatoxin B1 and Heavy Metal Contamination in Peanut and Peanut Soil in China during 2017–2018. *Food Control* **2020**, *118*, 107372. [[CrossRef](#)]

10. Lang, Q.Q.; Liu, Z.G.; Li, Y.F.; Xu, J.X.; Li, J.J.; Liu, B.S.; Sun, Q.P. Combustion Characteristics, Kinetic and Thermodynamic Analyses of Hydrochars Derived from Hydrothermal Carbonization of Cattle Manure. *J. Environ. Chem. Eng.* **2022**, *10*, 106938. [[CrossRef](#)]
11. Alves, J.L.F.; Da Silva, J.C.G.; Sellin, N.; Prá, F.D.B.; Sapelini, C.; Souza, O.; Marangoni, C. Upgrading of Banana Leaf Waste to Produce Solid Biofuel by Torrefaction: Physicochemical Properties, Combustion Behaviors, and Potential Emissions. *Environ. Sci. Pollut. Res.* **2022**, *29*, 25733–25747. [[CrossRef](#)] [[PubMed](#)]
12. Mahmood, H.; Shakeel, A.; Abdullah, A.; Khan, M.I.; Moniruzzaman, M. A Comparative Study on Suitability of Model-free and Model-fitting Kinetic Methods to Non-Isothermal Degradation of Lignocellulosic Materials. *Polymers* **2021**, *13*, 2504. [[CrossRef](#)]
13. Du, W.Z.; Wang, G.; Wang, Y.; Liu, X.L. Thermal Degradation of Bituminous Coal with Both Model-free and Model-fitting Methods. *Appl. Therm. Eng.* **2019**, *152*, 169–174. [[CrossRef](#)]
14. Vyazovkin, S.; Wight, C.A. Model-free and Model-fitting Approaches to Kinetic Analysis of Isothermal and Nonisothermal Data. *Thermochim. Acta* **1999**, *340*, 53–68. [[CrossRef](#)]
15. Torres-García, E.; Ramírez-Verduzco, L.F.; Aburto, J. Pyrolytic Degradation of Peanut Shell: Activation Energy Dependence on the Conversion. *Waste Manag.* **2020**, *106*, 203–212. [[CrossRef](#)] [[PubMed](#)]
16. Kumar, M.; Rai, D.; Bhardwaj, G.; Upadhyay, S.N.; Mishra, P.K. Pyrolysis of Peanut Shell: Kinetic Analysis and Optimization of Thermal Degradation Process. *Ind. Crop. Prod.* **2021**, *174*, 114128. [[CrossRef](#)]
17. Varma, A.K.; Singh, S.; Rathore, A.K.; Thakur, L.S.; Shankar, R.; Mondal, P. Investigation of Kinetic and Thermodynamic Parameters for Pyrolysis of Peanut Shell Using Thermogravimetric Analysis. *Biomass Convers. Biorefinery* **2020**, *12*, 4877–4888. [[CrossRef](#)]
18. Tao, W.M.; Zhang, P.; Yang, X.W.; Li, H.; Liu, Y.; Pan, B. An Integrated Study on the Pyrolysis Mechanism of Peanut Shell Based on the Kinetic Analysis and Solid/Gas Characterization. *Bioresour. Technol.* **2021**, *329*, 124860. [[CrossRef](#)]
19. Nie, Y.Z.; Deng, M.S.; Shan, M.; Yang, X.D. Evaluating the Impact of Wood Sawdust and Peanut Shell Mixing Ratio on Co-combustion Performance. *Fuel* **2022**, *324*, 124667. [[CrossRef](#)]
20. Xu, Z.H.; Xiao, X.; Fang, P.; Ye, L.M.; Huang, J.H.; Wu, H.W.; Tang, Z.J.; Chen, D.Y. Comparison of Combustion and Pyrolysis Behavior of the Peanut Shells in Air and N₂: Kinetics, Thermodynamics and Gas Emissions. *Sustainability* **2020**, *12*, 464. [[CrossRef](#)]
21. Torres-Sciancalepore, R.; Fernandez, A.; Asensio, D.; Riveros, M.; Fabani, M.P.; Fouga, G.; Mazza, G. Kinetic and Thermodynamic Comparative Study of Quince Bio-waste Slow Pyrolysis Before and After Sustainable Recovery of Pectin Compounds. *Energy Convers. Manag.* **2022**, *252*, 115076. [[CrossRef](#)]
22. Fernandez, A.; Palacios, C.; Echegaray, M.; Mazza, G.; Rodriguez, R. Pyrolysis and Combustion of Regional Agro-industrial Wastes: Thermal Behavior and Kinetic Parameters Comparison. *Combust. Sci. Technol.* **2017**, *190*, 114–135. [[CrossRef](#)]
23. Zalazar-Garcia, D.; Fernandez, A.; Cavaliere, L.; Deng, Y.; Soria, J.; Rodriguez, R.; Mazza, G. Slow Pyrolysis of Pistachio-waste Pellets: Combined Phenomenological Modeling with Environmental, Exergetic, and Energetic Analysis (3-E). *Biomass Convers. Biorefinery* **2022**, *14*, 9197–9215. [[CrossRef](#)]
24. Vyazovkin, S.; Sbirrazzuoli, N. Isoconversional Kinetic Analysis of Thermally Stimulated Processes in Polymers. *Macromol. Rapid Commun.* **2006**, *27*, 1515–1532. [[CrossRef](#)]
25. Brems, A.; Baeyens, J.; Beerlandt, J.; Dewil, R. Thermogravimetric Pyrolysis of Waste Polyethylene-terephthalate and Polystyrene: A Critical Assessment of Kinetics Modelling. *Resour. Conserv. Recycl.* **2011**, *55*, 772–781. [[CrossRef](#)]
26. Van de Velden, M.; Baeyens, J.; Boukis, I. Modeling CFB Biomass Pyrolysis Reactors. *Biomass Bioenergy* **2008**, *32*, 128–139. [[CrossRef](#)]
27. Van de Velden, M.; Baeyens, J.; Brems, A.; Janssens, B.; Dewil, R. Fundamentals, Kinetics and Endothermicity of the Biomass Pyrolysis Reaction. *Renew. Energy* **2010**, *35*, 232–242. [[CrossRef](#)]
28. GBT 212–2008; Proximate Analysis of Coal. Standardization Administration of China: China, 2008.
29. Sheng, C.D.; Azevedo, J.L.T.Á. Estimating the Higher Heating Value of Biomass Fuels from Basic Analysis Data. *Biomass Bioenergy* **2005**, *28*, 499–507. [[CrossRef](#)]
30. Kalak, T. Potential Use of Industrial Biomass Waste as a Sustainable Energy Source in the Future. *Energies* **2023**, *16*, 1783. [[CrossRef](#)]
31. Zhang, Y.Y.; Cuo, Y.X.; Cheng, F.Q.; Yan, K.Z.; Cao, Y. Investigation of Combustion Characteristics and Kinetics of Coal Gangue with Different Feedstock Properties by Thermogravimetric Analysis. *Thermochim. Acta* **2015**, *614*, 137–148. [[CrossRef](#)]
32. Deng, S.H.; Wang, X.B.; Tan, H.Z.; Mikulčić, H.; Yang, F.X.; Li, Z.F.; Duić, N. Thermogravimetric Study on the Co-combustion Characteristics of Oily Sludge with Plant Biomass. *Thermochim. Acta* **2016**, *633*, 69–76. [[CrossRef](#)]
33. Liu, X.; Chen, M.; Yu, D. Oxygen Enriched Co-combustion Characteristics of Herbaceous Biomass and Bituminous Coal. *Thermochim. Acta* **2013**, *569*, 17–24. [[CrossRef](#)]
34. Chen, J.B.; Mu, L.; Cai, J.C.; Yao, P.K.; Song, X.G.; Yin, H.C.; Li, A.M. Pyrolysis and Oxy-fuel Combustion Characteristics and Kinetics of Petrochemical Wastewater Sludge Using Thermogravimetric Analysis. *Bioresour. Technol.* **2015**, *198*, 115–123. [[CrossRef](#)] [[PubMed](#)]
35. Wang, G.W.; Zhang, J.L.; Shao, J.G.; Jiang, Y.K.; Gao, B.; Zhao, D.; Liu, D.H.; Wang, H.Y.; Liu, Z.J.; Jiao, K.X. Experiments and Kinetic Modeling for the Oxidative Decomposition of Herbaceous and Wooden Residues. *Bioresources* **2016**, *11*, 4821–4838. [[CrossRef](#)]
36. Tang, L.; Xiao, J.; Mao, Q.Y.; Zhang, Z.H.; Yao, Z.; Zhu, X.D.; Ye, S.C.; Zhong, Q.F. Thermogravimetric Analysis of the Combustion Characteristics and Combustion Kinetics of Coals Subjected to Different Chemical Demineralization Processes. *ACS Omega* **2022**, *7*, 13998–14008. [[CrossRef](#)]

37. Vyazovkin, S.; Chrissafis, K.; Di Lorenzo, M.L.; Koga, N.; Pijolat, M.; Roduit, B.; Sbirrazzuoli, N.; Suñol, J.J. ICTAC Kinetics Committee Recommendations for Collecting Experimental Thermal Analysis Data for Kinetic Computations. *Thermochim. Acta* **2014**, *590*, 1–23. [[CrossRef](#)]
38. Flynn, J.H. The “Temperature Integral”—Its Use and Abuse. *Thermochim. Acta* **1997**, *300*, 83–92. [[CrossRef](#)]
39. Ozawa, T.A. A New Method of Analyzing Thermogravimetric Data. *Bull. Chem. Soc. Jpn.* **1965**, *38*, 1881–1886. [[CrossRef](#)]
40. Ahmad, M.S.; Mehmood, M.A.; Ayed, O.S. Kinetic Analyses and Pyrolytic Behavior of Para Grass (*Urochloa Mutica*) for Its Bioenergy Potential. *Bioresour. Technol.* **2017**, *224*, 708–713. [[CrossRef](#)]
41. Alves, J.L.F.; Da Silva, J.C.G.; Da Silva Filho, V.F.; Alves, R.F.; Ahmad, M.S.; Ahmad, M.S.; Galdino, W.V.A.; De Sena, R.F. Bioenergy Potential of Red Macroalgae *Gelidium Floridanum* by Pyrolysis: Evaluation of Kinetic Triplet and Thermodynamics Parameters. *Bioresour. Technol.* **2019**, *291*, 121892. [[CrossRef](#)]
42. Chen, R.Y.; Li, Q.W.; Xu, X.K.; Zhang, D.D.; Hao, R.L. Combustion Characteristics, Kinetics and Thermodynamics of Pinus *Sylvestris* Pine Needle via Non-isothermal Thermogravimetry Coupled with Model-free and Model-fitting Methods. *Case Stud. Therm. Eng.* **2020**, *22*, 100756. [[CrossRef](#)]
43. Vyazovkin, S.; Burnham, A.K.; Criado, J.M.; Pérez-Maqueda, L.A.; Popescu, C.; Sbirrazzuoli, N. ICTAC Kinetics Committee Recommendations for Performing Kinetic Computations on Thermal Analysis Data. *Thermochim. Acta* **2011**, *520*, 1–19. [[CrossRef](#)]
44. Cai, H.M.; Zou, H.H.; Liu, J.Y.; Xie, W.M.; Kuo, J.H.; Buyukada, M.; Evrendilek, F. Thermal Degradations and Processes of Waste Tea and Tea Leaves via TG-FTIR: Combustion Performances, Kinetics, Thermodynamics, Products and Optimization. *Bioresour. Technol.* **2018**, *268*, 715–725. [[CrossRef](#)] [[PubMed](#)]
45. Cao, W.H.; Li, J.; Martí-Rosselló, T.; Zhang, X.L. Experimental Study on the Ignition Characteristics of Cellulose, Hemicellulose, Lignin and Their Mixtures. *J. Energy Inst.* **2019**, *92*, 1303–1312. [[CrossRef](#)]
46. Qiao, Y.Y.; Wang, B.; Ji, Y.Y.; Xu, F.; Zong, P.J.; Zhang, J.H.; Tian, Y.Y. Thermal Decomposition of Castor Oil, Corn Starch, Soy Protein, Lignin, Xylan, and Cellulose during Fast Pyrolysis. *Bioresour. Technol.* **2019**, *278*, 287–295. [[CrossRef](#)]
47. Vamvuka, D.; Sfakiotakis, S. Combustion Behaviour of Biomass Fuels and Their Blends with Lignite. *Thermochim. Acta* **2011**, *526*, 192–199. [[CrossRef](#)]
48. Çakman, G. Pyrolysis of *Euphorbia Rigida*: A Study on Thermal Characterizations, Kinetics, Thermodynamics via TG-FTIR Analysis. *J. Environ. Manag.* **2024**, *357*, 120835. [[CrossRef](#)] [[PubMed](#)]
49. Yu, D.; Chen, M.Q. Oxygen Enriched Co-combustion of Biomass and Bituminous Coal. *Energy Sources Part A Recovery Util. Environ. Eff.* **2016**, *38*, 994–1001. [[CrossRef](#)]
50. Jia, G.H. Combustion Characteristics and Kinetic Analysis of Biomass Pellet Fuel Using Thermogravimetric Analysis. *Processes* **2021**, *9*, 868. [[CrossRef](#)]
51. Liao, X.J.; Singh, S.; Yang, H.P.; Wu, C.F.; Zhang, S.H. A Thermogravimetric Assessment of the Tri-combustion Process for Coal, Biomass and Polyethylene. *Fuel* **2021**, *287*, 119355. [[CrossRef](#)]
52. Mureddu, M.; Dessi, F.; Orsini, A.; Ferrara, F.; Pettinau, A. Air-and Oxygen-blown Characterization of Coal and Biomass by Thermogravimetric Analysis. *Fuel* **2018**, *212*, 626–637. [[CrossRef](#)]
53. Jiang, L.; Zhang, D.; Li, M.; He, J.J.; Gao, Z.H.; Zhou, Y.; Sun, J.H. Pyrolytic Behavior of Waste Extruded Polystyrene and Rigid Polyurethane by Multi Kinetics Methods and Py-GC/MS. *Fuel* **2018**, *222*, 11–20. [[CrossRef](#)]
54. Xu, X.K.; Pan, R.M.; Chen, R.Y. Combustion Characteristics, Kinetics, and Thermodynamics of Pine Wood Through Thermogravimetric Analysis. *Appl. Biochem. Biotech.* **2021**, *193*, 1427–1446. [[CrossRef](#)] [[PubMed](#)]
55. Zhao, Z.Y.; Liu, P.H. Combustion Characteristics and Kinetics of Five Tropic Oilgal Strains Using Thermogravimetric Analysis. *J. Therm. Anal. Calorim.* **2018**, *131*, 1919–1931. [[CrossRef](#)]
56. Yiga, V.A.; Katamba, M.; Lubwama, M.; Adolfsson, K.H.; Hakkarainen, M.; Kamalha, E. Combustion, Kinetics and Thermodynamic Characteristics of Rice Husks and Rice Husk-biocomposites Using Thermogravimetric Analysis. *J. Therm. Anal. Calorim.* **2023**, *148*, 11435–11454. [[CrossRef](#)]
57. Chong, C.T.; Mong, G.R.; Ng, J.H.; Chong, W.W.F.; Ani, F.N.; Lam, S.S.; Ong, H.C. Pyrolysis Characteristics and Kinetic Studies of Horse Manure using Thermogravimetric Analysis. *Energy Convers. Manag.* **2019**, *180*, 1260–1267. [[CrossRef](#)]
58. Ahmad, M.S.; Mehmood, M.A.; Taqvi, S.T.H.; Elkamel, A.; Liu, C.G.; Xu, J.; Rahimuddin, S.A.; Gull, M. Pyrolysis, Kinetics Analysis, Thermodynamics Parameters and Reaction Mechanism of Typha *Latifolia* to Evaluate Its Bioenergy Potential. *Bioresour. Technol.* **2017**, *245*, 491–501. [[CrossRef](#)]
59. Patidar, K.; Singathia, A.; Vashishtha, M.; Sangal, V.K.; Upadhyaya, S. Investigation of Kinetic and Thermodynamic Parameters Approaches to Non-isothermal Pyrolysis of Mustard Stalk using Model-free and Master Plots Methods. *Mater. Sci. Energy Technol.* **2022**, *5*, 6–14. [[CrossRef](#)]
60. Petrovič, A.; Vohl, S.; Cenčič Predikaka, T.; Bedoič, R.; Simonič, M.; Ban, I.; Čuček, L. Pyrolysis of Solid Digestate from Sewage Sludge and Lignocellulosic Biomass: Kinetic and Thermodynamic Analysis, Characterization of Biochar. *Sustainability* **2021**, *13*, 9642. [[CrossRef](#)]

Disclaimer/Publisher’s Note: The statements, opinions and data contained in all publications are solely those of the individual author(s) and contributor(s) and not of MDPI and/or the editor(s). MDPI and/or the editor(s) disclaim responsibility for any injury to people or property resulting from any ideas, methods, instructions or products referred to in the content.